Bull. Chem. Soc. Ethiop. **2025**, 39(6), 1213-1226.
DOI: https://dx.doi.org/10.4314/bcse.v39i6.15

ISSN 1011-3924
Printed in Ethiopia
Online ISSN 1726-801X
© 2025 Chemical Society of Ethiopia and The Authors

KINETICS, ISOTHERMS AND THERMODYNAMICS STUDY OF EOSIN YELLOW DYE ADSORPTION FROM AQUEOUS SOLUTIONS BY MnO_2@rGO NANOCOMPOSITE

Esraa Saleh Alwan, Faiq F. Karam* and, Zeina M. Kadam

Department of Chemistry, College of Sciences, University of Al-Qadisiyah, Iraq

(Received July 24, 2024; Revised December 27, 2024; Accepted February 25, 2025)

ABSTRACT. This study explores the use of MnO_2@rGO nanocomposite as an adsorbent for Eosin Y dye. It was found that equilibrium for Eosin Y adsorption on the MnO_2@rGO nanocomposite surface is achieved in 120 min. The nanocomposite demonstrated a high dye adsorption rate due to its extensive surface area, which facilitates substantial dye uptake. To assess the adsorption kinetics of Eosin Y on the MnO_2@rGO surface; the data suggested that the pseudo-second-order model fit the data better. The Langmuir, Freundlich, and Temkin equations are examples of linear forms of adsorption isotherms that were investigated in this study and the substantial correlation coefficient for the Freundlich isotherm model suggests that the adsorption of Eosin Y dye on the MnO_2@rGO nanocomposite surface is multilayered. Furthermore, the effects of pH, ionic strength, and thermodynamic factors on maximum adsorption were examined. In addition, thermodynamic functions including entropy (ΔS), enthalpy (ΔH), and Gibbs free energy (ΔG) were evaluated and the adsorption is physical.

KEY WORDS: MnO_2@rGO nanocomposite, Eosin yellow dye, Adsorption, Adsorption isothermal, Characterization, Thermodynamics, kinetics

INTRODUCTION

An abundance of interest has been generated by the possibility of dye adsorption onto nanocomposite surfaces for environmental remediation [1-3]. Eosin Y dye is widely used in various areas; however, because of its toxicity and durability, it poses a threat to the environment [4-6]. When reduced graphene oxide (rGO) and manganese dioxide (MnO_2) are combined, a nanocomposite (MnO_2@rGO) with remarkable adsorption properties is produced [7-8]. MnO_2 and rGO work synergistically to create a composite material with a wide surface area, enhanced adsorption capacity, and greater chemical stability. This makes it a suitable choice for removing dye from aqueous solutions [9]. The MnO_2@rGO nanocomposite exhibits unique properties as a result of the combination of MnO_2 catalytic properties and rGO large surface area and excellent electrical conductivity. These features make it possible for Eosin Y dye molecules to be quickly removed from contaminated water by efficient adsorption [10, 11]. Studies have revealed that the adsorption kinetics of Eosin Y on MnO_2@rGO follow pseudo-second-order models, indicating that chemisorption is the primary mechanism [12]. This suggests a strong connection between the dye molecules and the active spots on the nanocomposite's surface. Adsorption isotherms like the Langmuir and Freundlich models have been utilized in addition to kinetic studies [13] to understand the adsorption behavior and capacity of MnO_2@rGO. Entropy, Gibbs free energy, and enthalpy are thermodynamic metrics that shed light on the feasibility and spontaneity of the adsorption process [14, 15]. MnO_2@rGO's adaptability and endurance to a variety of environmental conditions are demonstrated by the effects of pH and ionic strength on its adsorption capacity [16, 17]. Consequently, the water-based adsorption of Eosin Y dye presents a prospective treatment for which the MnO_2@rGO nanocomposite may be useful [18, 19]. Its

*Corresponding authors. E-mail: faiq.karam@qu.edu.iq
This work is licensed under the Creative Commons Attribution 4.0 International License

excellent adsorption kinetics and isothermal behaviors, along with its high efficiency, demonstrate its prospective applications in wastewater treatment and environmental protection [20, 21]. More research aimed at enhancing MnO_2@rGO production and functionalization could lead to dye removal methods that are even more effective and long-lasting [22]. Sustainable energy is expressed by the transition from fossil fuels to renewable energy sources is a significant global challenge that necessitates technological improvements in systems, tools, and materials to enable efficient harvesting, storing, converting, and managing renewable energy. In an effort to accelerate these developments, energy experts have begun utilizing machine learning (ML) techniques. The energy transition's two primary objectives are lowering the use of fossil fuels and making sure that harmful environmental repercussions are adequately mitigated. In certain economies, implementing the energy transition might be difficult due to the integration of social, political, economic, and, finally, technological components. The rapid speed at which digital transformation has occurred has made it feasible to implement a range of astute technical solutions in a focused way that can expedite the accomplishment of significant energy transition objectives [23] carried out research of this work is to create multi-walled carbon nanotube acid (M WCNTs-COOH) by grafting CNTS with chitosan (CS) and employing the fragment flam deposition technique (FFD) to create a composite material called CS-OMWCNTs. The active groups, such as COOH and OH that are present on the surface of carbon nanotubes were revealed by FT-IR. [24] Conducted a study the synthesis and characterization of a new heterocyclic azo – azo methine ligand and its application of ferrous in some drugs. Azo2-((E)–(1H-benzo[d]imidazol-2- yl)diazinyl)-5-(E-4-(dimethyl amino) benzylidene amino) phenol, (BIADMebP) has been synthesized from condensation reaction of 2-[(-2-benzimidazolyl) azo]-5-amino phenol with N,N-dimethyl benzaldehyde. The stability constants for these complexes have been calculated spectrally by UV-Visible spectra. All results show that these complexes have high stability [25] carried out research utilizing a novel azo reagent; a novel heterocyclic organic ligand was created, and it was then examined utilizing organic diagnostic techniques like UV-Vis, and FT-IR. The wavelength at which the biggest absorption peak was seen was 620 nm. The wavelength of the reagent, however, was 475 nm. At longer wavelength ranges, the linear range was between concentration and absorption: 0.3–20 $mg.L^{-1}$ [26] carried out research. Under specific circumstances, the adsorption of Mebeverine hydrochloride (MB.HCl) on chitosan polymer was investigated. From the starting pH of 1.1, chitosan adsorption increased, and over the pH range of 2–10, it dropped. At every temperature examined, the result of (ΔG) is negative, indicating a spontaneous tendency for MB.HCl to adsorb onto chitosan. As the temperature increased from 5 °C to 25 °C, the value of (ΔG) decreased, suggesting that MB.HCl would adsorb more readily at a higher temperature [27] carried out research. The novel organic azo reagent dye was used in this work to prepare a number of metal complexes. The UV-Visible and FT-IR spectra were used to diagnose these lectured complexes. Its geometric shape is octahedral [28] carried out research. In this work, polyacryl amid-co-maleic acid is used as an efficient adsorbent for atenolol adsorption from an aqueous solution. Batch tests are conducted to examine the effects of various parameters on the drug's adsorption process, including contact time, adsorbent weight, temperature, pH, and ionic intensity. Drug was removed from an aqueous solution in 94.2% of cases, and the adsorption process followed the second pseudo-order ($R^2 = 0.999$). According to the adsorption isotherm, the Timken and Freund models were used in the adsorption process. Adsorption is a non-spontaneous and exothermic process that is shown by the calculation of thermodynamic functions. The aim of this research is to better understand the adsorption mechanisms, determine the optimal operating conditions to achieve maximum eosin dye removal efficiency, and investigate the kinetics, thermodynamics and isotherms of the aspirin adsorption process using MnO_2@rGO nanocomposite. This will allow evaluating the effectiveness of this method for treating water contaminated with eosin dye.

EXPERIMENTAL

Materials

Graphene oxide (GO), potassium chloride (KCl), sodium chloride (NaCl), calcium carbonate ($CaCO_3$), ethanol, eosin Y, hydrochloric acid (HCl), hydrazine and potassium permanganate ($KMnO_4$) completely pure reagents were utilized, and all solutions were made using deionized water.

Preparation of MnO_2@rGO nanocomposite

MnO_2 and the MnO_2@rGO nanocomposite were produced using a hydrothermal method. First, a few drops of HCl were added to 25 mL of distilled water that had 3.5 mmol of $KMnO_4$ dissolved in it. This mixture was given a stirrer at 25 ºC. In the meantime, a sonication bath was used to disperse 50 mg of GO in 10 mL of distilled water that included hydrazine. After that, the $KMnO_4$ solution and the GO dispersion were mixed and stirred at room temperature for half an hour. Once the mixture was transferred to a 100-mL hydrothermal autoclave featuring a Teflon lining, it was heated to 140 °C for a duration of 12–14 hours. After the reaction was complete and the mixture had cooled to room temperature, the final product was separated using centrifugation. The product was thoroughly cleaned in ethanol and deionized water, and then it was let to dry overnight at 70 °C [29].

Adsorption studies

These experiments aim to investigate the effects of temperature (15, 20, 25, and 30 ºC) and adsorption quantity, as well as the effects of time, to determine the ideal pH and contact time of the eosin dye solution. To comprehend the eosin dye adsorption process on the surface of the MnO_2@rGO adsorbent, additional research is being done on the effects of temperature lines, adsorption kinetics, and ionic intensity. In order to ascertain the dye's maximal adsorption, a set quantity of nanocomposite (0.05 g) was combined with 10 mL of dye solution and put inside a shaking apparatus. Dyes concentrations were determined using ultraviolet-visible spectroscopy equipment. The quantum of dye absorbed on the nanocomposite surface was computed [30, 31] by employing the subsequent mathematical formula:

$$Q_e = \frac{V_{sol}(C_o - C_e)}{m} \quad (1)$$

where the quantity of adsorbate adsorbed per mass of adsorbent is known as Q_e, and it is measured in $mg.g^{-1}$, C_o is the initial (in $mg.L^{-1}$) concentration of the adsorbate in the solution. C_e represents the adsorbate's equilibrium concentration in milligrams per liter of solution. V is the solution's volume (L), the mass of the adsorbent is represented by the symbol m (g). The adsorption capacity could be precisely calculated according to this formula, which also made it easier to analyze the many elements influencing the adsorption effectiveness.

Fourier transform infrared spectroscopy

The functional groups that are involved in the composition of the Mno_2@rGO nanocomplex were identified using Fourier transform infrared spectroscopy (FT-IR). The potassium bromide (KBr) disc method was used to obtain the complex's FTIR spectra, which were obtained within a range of wavenumbers 400–4000 cm^{-1}.

RESULTS AND DISCUSSION

Characterization of the MnO_2@rGO nanocomposite

Characteristic peaks related to the materials involved in the creation of the composite may be seen in the FT-IR spectra of the MnO_2@rGO nanocomposite, as illustrated in Figure 1(a). These peaks are indicative of Mn-O stretching oscillations, which arise because of carbon dioxide and appear in the 500–700 cm^{-1} range. Mandarin. Furthermore, the presence of OH stretching vibrations corresponding to hydroxyl groups is indicated by the large peak in the 3200-3600 cm^{-1} region. Reduced graphene oxide (rGO) is characterized by peaks at 1600 cm^{-1} that are caused by C=C stretching vibrations found in the graphene's aromatic carbon-carbon bonds, and peaks in the range of 1700–1750 cm^{-1} that are caused by C=O stretching vibrations [32].

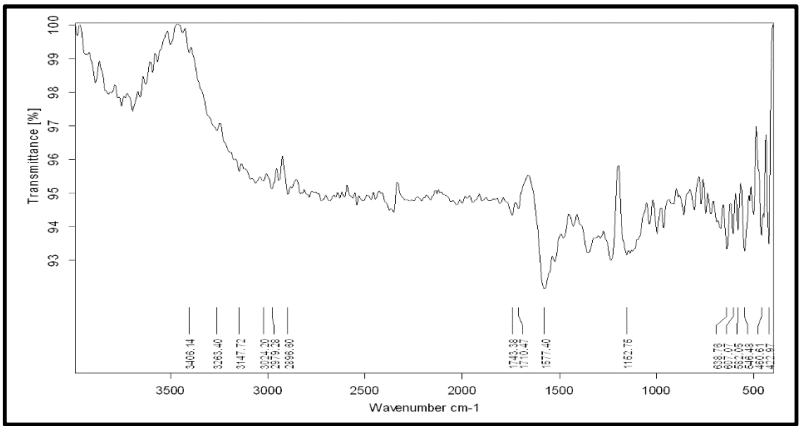

Figure 1(a). The MnO_2@rGO nanocomposite's FTIR spectrum prior to Eosin Y adsorption.

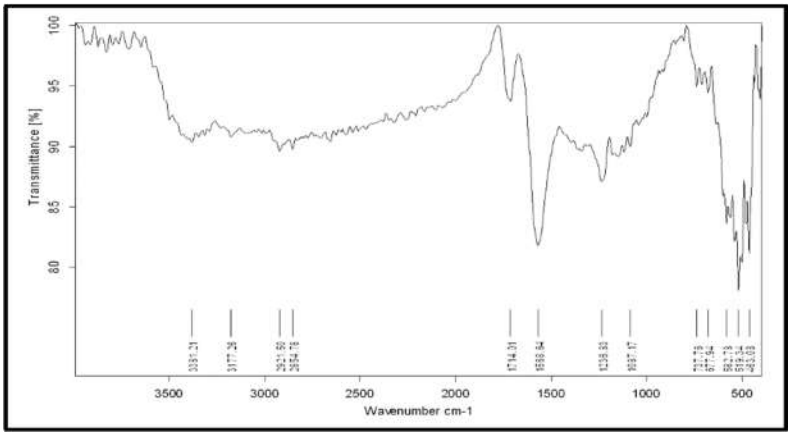

Figure 1(b). The MnO_2@rGO nanocomposite's FTIR spectrum following aspirin adsorption.

After the Eosin dye was adsorbed, Figure 1(b) displays the composite's FT-IR spectrum changed as a result of it. Manganese dioxide is responsible for the Mn-O stretching peaks in the region of 500–700 cm^{-1}, which are a result of the interaction between the dye molecules and the composite surface. It implies that it takes part in the process of adsorption. Additionally, there are peaks that seem to be associated with the sulfonate groups (SO_3^-) and aromatic expansion groups C=C, which suggest that the dye has been adsorbed on the composite's surface. The peaks that occur within the range 3200–3600 cm^{-1} are due to the intensity of the OH expansion vibrations, and the peaks that appear within the range 1700–1750 cm^{-1} are due to the C=O expansion vibrations. However, the peaks associated with groups containing oxygen may decrease or change due to their influence on the adsorption process. O, and this shows that these groups take part in adsorption. The creation of bonds between the dye molecules and the nanocomposite is responsible for the peaks that show up in the 1000–1400 cm^{-1} area [33-35].

The effect of time

Looked at how long it takes for the Eosin Y dye to adsorb on the MnO_2@rGO nanocomposites' adsorbent surface. It was discovered that the longer the solution is in contact with the adsorbed portion of the surface, the greater the surface's capacity to adsorb. As a result, as Figure 2 [36-37] illustrates, the amount of adsorbed dye rises with time.

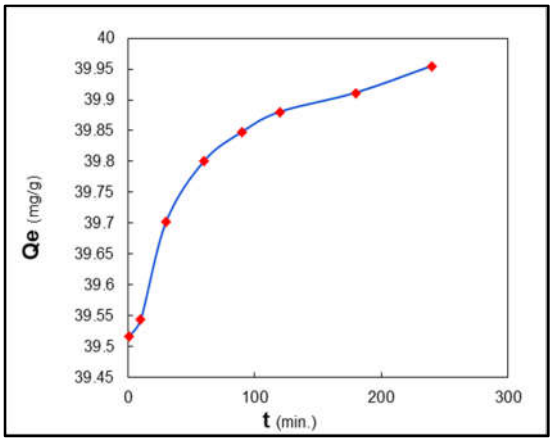

Figure 2. The impact of varying the Eosin Y dye adsorption period at 120 min, 25 °C, 0.05 g of MnO_2@rGO in (10 mL) of dye (200 mg/L), and pH = 7 on the adsorbent surface.

Adsorption of the dye Eosin Y

To explain the dye adsorption process at 25 °C, the concentration of Eosin Y dye was plotted against the amount of adsorbent used. Due to the active functional groups that encourage dye adsorption, the MnO_2@rGO nanocomposite surface's adsorption capability is shown in Figure 3. There was a noticeable high dye adsorption efficacy on the surface, indicating a substantial interaction between the dye molecules and the adsorbent. The great adsorption capacity of the MnO_2@rGO nanocomposite is due to its large surface area and abundance of active sites, which enhance the adsorption process by providing the dye molecules with more binding sites [38-39].

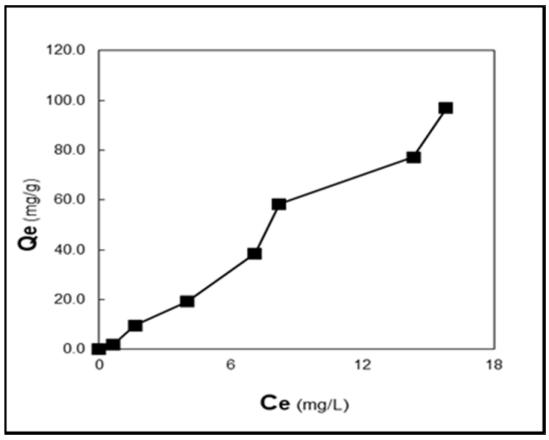

Figure 3. The Eosin Y dye adsorption isotherm at 25 °C, pH = 7, and 120 min.

Adsorption isothermal of Eosin Y

The interaction between dye molecules and MnO_2@rGO was studied at 25 °C by analyzing the adsorption process using Freundlich, Langmuir, and Temkin isotherm models. The adsorption behavior of Eosin Y was best represented by the isothermal Freundlich model, as shown in Figures 4(a), (b) and (c) indicating multilayer adsorption on a heterogeneous surface [40]. Adsorption occurs on a surface where the distribution of adsorption heat and coefficients is irregular, as indicated by the Freundlich isotherm. The results were inconsistent with the Langmuir isotherm, which relies on the supposition of monolayer adsorption occurring on a uniform surface. This implies that there is heterogeneity among the adsorption sites on the MnO_2@rGO nanocomposite. The Temkin isotherm provided information on the adsorption process even though it was less accurate than the Freundlich model because it considered the impact of indirect interactions between the adsorbent and the adsorbate. The substantial correlation coefficient for the Freundlich isotherm model [41] suggests that the adsorption of Eosin Y dye on the MnO_2@rGO nanocomposite surface is multilayered shown in Figures 4(a), (b) and (c) the results showed that the adsorption process is identical to the (S) class according to the Giles Classification. This indicates that the adsorption is multilayered and the orientation of the adsorbent materials on the adsorbent surface is oblique or perpendicular to the adsorbent surface. The solvent may suffer from strong adsorption on the adsorbent surface, using the Langmuir, Freundlich, and Temkin equations and takes place on a heterogeneous surface with varying affinities for the dye molecules. The results shown in Table 1 showed the application of the Freundlich isotherm shows that the adsorption is multilayer, indicating the heterogeneous nature of the surface and that the active sites on the surface of the nanocomposite are of unequal energy.

Table 1. Correlation coefficients, Langmuir, Freundlich and Temkin isotherms constants and adsorption capacity of the dyes Eosin Y adsorbed on the surface of prepared MnO_2@rGO nanocomposite.

Langmuir equation			Freundlich equation			Temkin equation		
K_L	q_m	R^2	K_F	N	R^2	K_T	B	R^2
0.0575	4.1701	0.4275	4.0364	0.85579	0.9814	0.9683	27.633	0.8299

Effects of thermodynamics

The thermodynamic study showed that raising the temperature increases the MnO_2@rGO nanocomposite's ability to adsorb. As seen in (Figure 5), this rise suggests that the adsorption process is endothermic. Increased temperature causes the solution's viscosity to decrease, facilitating more effective diffusion of the adsorbate molecules over the adsorbent surface. A temperature-dependent rise in kinetic energy is observed in the adsorbate molecules. With more kinetic energy, there is a greater chance that the molecules of the adsorbate will interact with the active sites on the adsorbent surface, allowing for more adsorption. In addition to helping molecules pass through activation energy barriers and bind to available active sites, rising temperatures can also facilitate the entry of more molecules into the pore-forming adsorbent material [42].

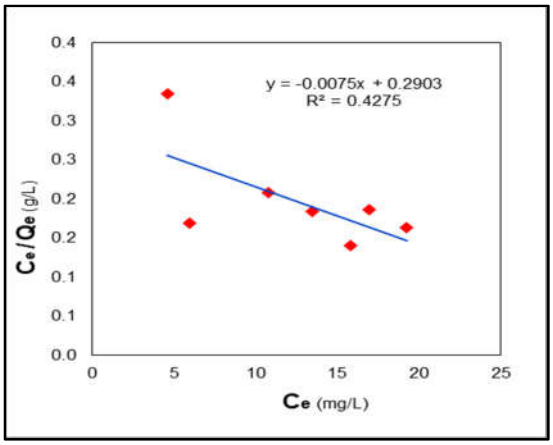

Figure 4(a). The Langmuir isotherm for the adsorption of Eosin Y dye on the MnO_2@rGO surface.

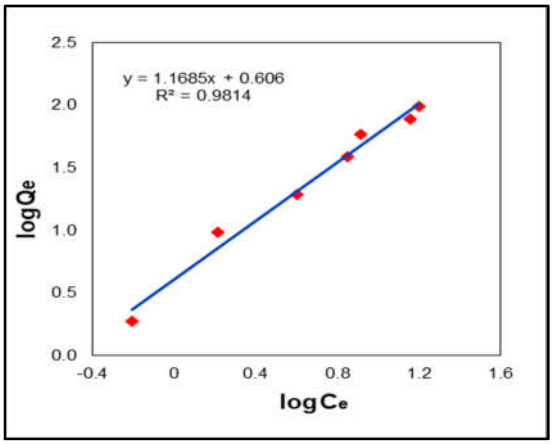

Figure 4(b). The Freundlich isotherm for the adsorption of Eosin Y dye on the MnO_2@rGO surface.

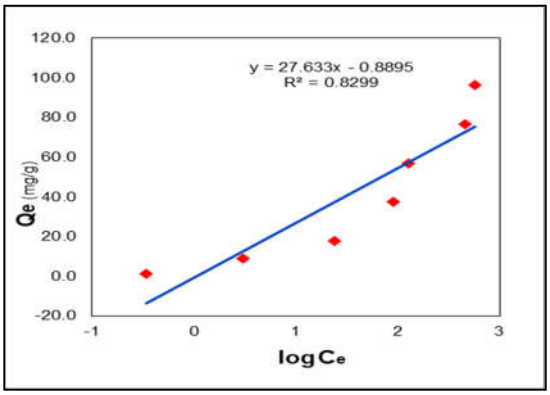

Figure 4(c). The Timken isotherm for the adsorption of Eosin Y dye on the MnO_2@rGO surface.

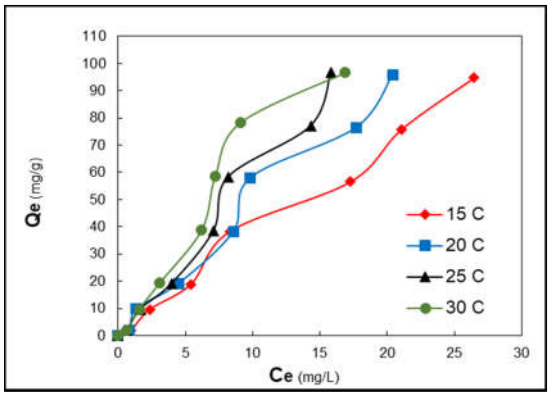

Figure 5. The amount of Eosin Y dye absorbed at different temperatures at the surface of MnO_2@rGO.

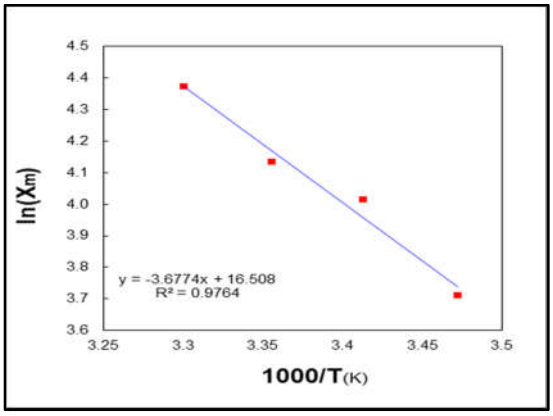

Figure 6. The plot of ln Xm against the absolute temperature of the adsorption of eosin y dye on the MnO_2@rGO surface.

$$\ln Xm = \frac{-\Delta H}{RT} + \text{constant} \quad (2)$$

$$\Delta G^{o} = -RT \ln k_{eq} \quad (3)$$

$$\Delta S = \frac{\Delta H - \Delta G}{T} \quad (4)$$

The calculated thermodynamic properties, which include variations in free energy (ΔG), enthalpy (ΔH), and entropy (ΔS). The findings imply an endothermic adsorption process since equilibrium constant (k_{eq}) = 33.24 and there is a positive enthalpy change (ΔH = 30.57 (kJ.mol^{-1}). This indicates that heat from the environment must be absorbed by the MnO_2@rGO nanocomposite in order for the Eosin Y dye to adsorb onto it. This heat requirement rises with temperature. Free energy change (ΔG) = -23.47 (kJ.mol^{-1}) values in the negative range indicate the spontaneity of the adsorption process. When the ΔG value is negative, it means that the adsorption process happens naturally in the given circumstances, which makes the MnO_2@rGO nanocomposite a good adsorbent for Eosin Y dye. Additionally, a rise in irregularities at the solid-liquid interface throughout the adsorption process is indicated by the positive entropy (ΔS) change = 181.35 (J.mol^{-1}. K^{-1}). This is explained by the dye molecules' larger kinetic energy at higher temperatures, which increases their mobility and causes them to interact with the adsorbent's active sites in a more disordered form. The more effectively the dye molecules disperse throughout the adsorbent surface and inside its pores, the more unpredictability that results [43-44]. The adsorption is physical, as indicated by the value of (ΔH = 30.57 (kJ.mol^{-1}).

The effect of ionic strength

An important factor influencing the adsorption processes is ionic strength. The solubility of the dye decreases as the concentration of salt in the solution rises due to the reaction between the solvent molecules and salt ions. This results in more dye being adsorbed on the surface of the adsorbent, as shown in Figure 7. This results in more dye being adsorbed on the surface of the adsorbent. Salt ions in the solution enhance dye molecule adsorption by fortifying the ionic strength of the double layer around the adsorbent surface. An important part of this process is the fight between the dye and salt ions for interaction with the solvent molecules. By interacting with the solvent, salt ions efficiently decrease the solubility of dye molecules, increasing their propensity to adsorb onto the surface of the MnO_2@rGO nanocomposite. This process, called the "salting-out effect," occurs when salts are present because they cause dye molecules to aggregate and become more easily absorbed by the adsorbent material [45-46].

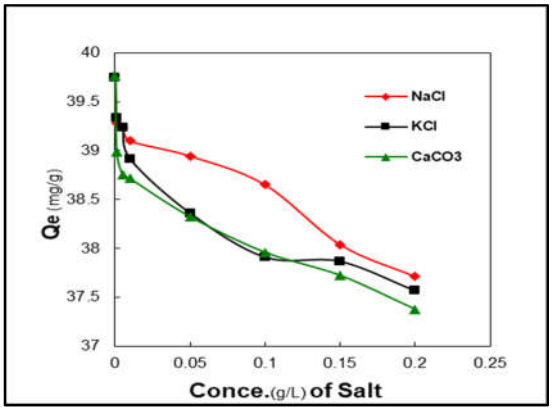

Figure 7. The salt effects on the adsorption of Eosin Y dye on the MnO_2@rGO surface.

Kinetics of adsorption

The adsorption kinetics of the dye Eosin Y on the surface of the MnO_2@rGO nanocomposite were investigated using two kinetic models: the pseudo-first-order and the pseudo-second-order equations [47].

$$\ln (q_e - q_t) = \ln q_e - k_1 t \quad (5)$$

$$\frac{t}{q_t} = \frac{1}{k_2 q_e^2} + \frac{1}{q_e} t \quad (6)$$

Applying these models to a review of the empirical information results in greater correlation coefficients (R^2) between the pseudo-second-order kinetic model and the observed dye adsorption kinetics, as Figure 8(a and b) illustrate. The number of vacant sites and the pace at which adsorption sites are occupied are said to be proportional, according to the pseudo-first-order kinetic model. The adsorption kinetics of dyes on heterogeneous surfaces, where several adsorption sites and processes may be involved, are frequently difficult for this model to adequately describe. However, the pseudo-second-order kinetic method, which suggests that the method of adsorption depends on the square of the number of empty sites, is better supported by the experimental results in this work. This idea suggests that physical adsorption, a process that uses valence forces through the passing on or trading of electrons with the adsorbent and adsorbate, is most likely the phase that limits the rate. Based on the improved fit of the pseudo-second-order model, the adsorption of Eosin Y dye on the surface of the MnO_2@rGO nanocomposite is likely more intricate and involves chemical interactions. Determining the optimal conditions for maximal dye removal effectiveness and comprehending the adsorption mechanism depend heavily on this discovery [48].

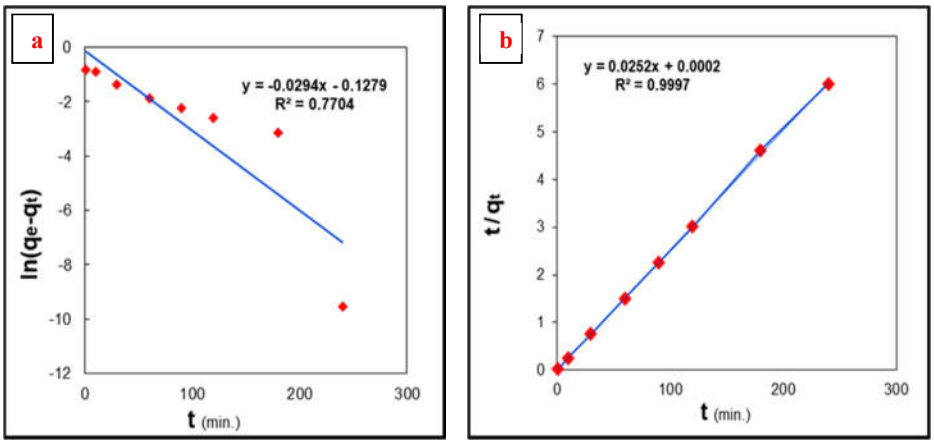

Figure 8. The pseudo-first-order model (a) and pseudo-second-order model (b) of the adsorption of Eosin Y dye on MnO_2@rGO.

The pH effect

Figure 9 shows how the study's findings on the effect of solution pH on the MnO_2@rGO nanocomposite's adsorption capability. The quantity of Eosin Y dye adsorbed on the surface of the nanocomposite was found to be influenced by acidity or alkalinity, as tested by the study throughout a pH range of 2 to 10. For one hundred and 120 min, at room temperature, a solution

comprising 0.05 g of MnO_2@rGO composite and 200 mg.L^{-1} of Eosin Y dye was combined. UV-Vis spectroscopy was used to assess the dye content in the supernatant after the mixtures were centrifuged following the adsorption procedure. The adsorption capacity changed greatly with pH, according to the data. The surface of MnO_2@rGO contains functional groups (such as -OH) that can be ionized depending on the pH value. At low pH, the surface is positively charged due to the protonation of functional groups, which attracts the negatively charged (anionic) dye. With increasing pH, the surface charge becomes negative due to the deprotonation, which leads to repulsion between the surface and the negatively charged dye [49-50].

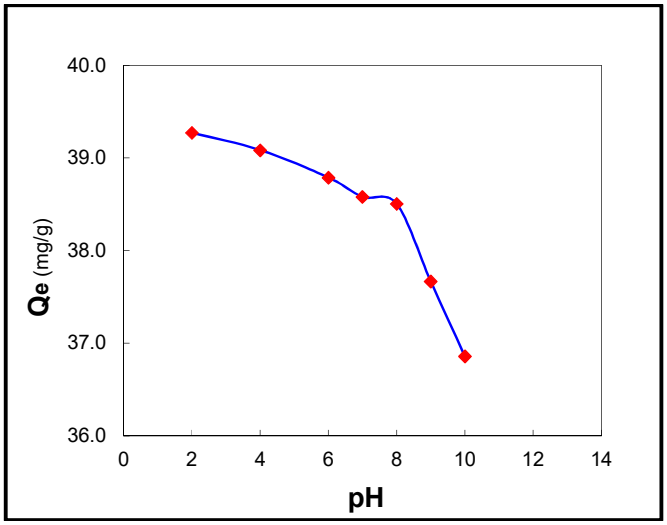

Figure 9. Effect of pH on Eosin Yellow adsorption.

CONCLUSIONS

The MnO_2@rGO nanocomposite was utilized as an adsorbent in the investigation to remove Eosin Y dye. FTIR was employed to describe the artificial nanocomposite. It was shown that several factors influenced the composite's adsorption capacity, including temperature, solution pH, ionic strength, and contact time. Ionic strength, and contact duration, affected the composite ability to adsorb. The adsorption behavior suggested a heterogeneous surface adsorption process and was in line with Freundlich's isotherm model. To further comprehend the viability and spontaneity of the adsorption process, thermodynamic parameters including entropy (ΔS), enthalpy (ΔH), and Gibbs free energy (ΔG) were examined. These specifications are useful. Pseudo-second-order model adsorption kinetics indicate that physical adsorption via electron sharing or transfer the phase that restricts the rate could involve the adsorbent and the adsorbate. In order to comprehend the viability and spontaneity of the adsorption process, the maximal adsorption capacity and the type of interactions involved may be ascertained with the use of these factors.

REFERENCES

1. Mok, C.; Ching, Y.; Muhamad, F.; Abu Osman, N.; Hai, N.; Che, H.; Che, R. Adsorption of dyes using poly (vinyl alcohol) (PVA) and PVA-based polymer composite adsorbents: A review. *J. Environ. Polym. Degrad.* **2020**, 28, 775-793.

2. Karam, F.; Fatima F.; Haider M. Adsorption of toxic crystal violet dye using (Chitosan-OMWCNTs) from aqueous solution. *J. Phys. Conf. Ser*. **2021**, 1999, 012015.
3. Yilmaz, M.; Kocyigit, A.; Aydogan, S.; Incekara, U.; Sahin, Y.; Kacus, H. Influence of illumination intensity on electrical characteristics of Eosin y dye-based hybrid photodiode: comparative study. *Appl. Phys. A* **2020**, 126, 1-12.
4. Chen, L.; Yin, H.; Zhang, Y.; Xie, H. Facile synthesis of modified MnO_2/reduced graphene oxide nanocomposites and their application in supercapacitors. *Nano.* **2020**, 15, 2050099.
5. Rashak, A.; Faiq, F. Preparation of graphene oxide and multi-walled carbon nanotubes, and they are used to modify the glassy carbon electrode for sensing enalapril maleate. *Results Chem*. **2024**, 8, 101597.
6. Xie, A.; Wang, H.; Zhu, Z.; Zhang, W.; Li, X.; Wang, Q.; Luo, S. Mesoporous CeO_2-α-MnO_2-reduced graphene oxide composite with ultra-high stability as a novel electrode material for supercapacitor. *Surf. Interfaces* **2021**, 25, 101177.
7. Sakr, M.; Adly, M.; Gar Alalm, M.; Mahanna, H. Effective removal of acetamiprid and eosin Y by adsorption on pristine and modified MIL-101 (Fe). *ESPR* **2024**, 31, 1-25.
8. Rashtbari, Y.; Afshin, S.; Hamzezadeh, A.; Gholizadeh, A.; Ansari, F.; Poureshgh, Y.; Fazlzadeh, M. Green synthesis of zinc oxide nanoparticles loaded on activated carbon prepared from walnut peel extract for the removal of Eosin Y and Erythrosine B dyes from aqueous solution: Experimental approaches, kinetics models, and thermodynamic studies. *ESPR*. **2022**, 29, 1-13.
9. Alwan, A.; Jasim, L.; Sahib, I. Synthesis and characterization of graphene oxide-(carboxymethylcellulose-sodium alginate-acrylic acid) hydrogel composite for Azure B removal from aqueous solutions. *AIP Conf. Proc.* **2023**, 2977, 040001.
10. Al-Madani, M.; Salah, A.; Faraj, M. Thermodynamics, isotherms, and kinetics evaluation of the (nickel oxide/cerium dioxide/graphene oxide nanocomposite) for methylene blue (MB) dye removal. *AJAPAS* **2024**, 183-196.
11. Shahwan, T. Critical insights into the limitations and interpretations of the determination of ΔG^o, ΔH^o, and ΔS^o of sorption of aqueous pollutants on different sorbents. *J. Colloid Interface Sci*. **2021**, 41, 100369.
12. Al-Ghouti, M.; Rana, S. Mechanistic understanding of the adsorption and thermodynamic aspects of cationic methylene blue dye onto cellulosic olive stones biomass from wastewater. *Sci. Rep*. **2020**, 10, 15928.
13. Hu, R.; Wang, W.; Tan, J.; Chen, L.; Dick, J.; He, G. Mechanisms of shale gas adsorption: Insights from a comparative study on a thermodynamic investigation of microfossil-rich shale and non-microfossil shale. *Chem. Eng. J*. **2021**, 411, 128463.
14. Yang, R.; Fan, Y.; Ye, R.; Tang, Y.; Cao, X.; Yin, Z.; Zeng, Z. MnO_2-based materials for environmental applications. *J. Adv. Mater.* **2021**, 33, 2004862.
15. Elsehsah, K.; Zulkarnain, A.; Norhafezaidi, M. Graphene aerogel electrodes: A review of synthesis methods for high-performance supercapacitors. *J. Energy Storage*. **2024**, 97, 112788.
16. Kanwal, T.; Rasheed, S.; Hassan, M.; Fatima, B.; Xiao, H.; Musharraf, S.; Najam-ul-Haq, M.; Hussain, D. Smartphone-assisted EY@ MOF-5-based dual-emission fluorescent sensor for rapid on-site detection of daclatasvir and nitenpyram. *ACS Appl. Mater. Interfaces* **2023**, 16, 1688-1704.
17. Purkait, M.; DasGupta, S.; De, S. Adsorption of eosin dye on activated carbon and its surfactant based desorption. *Environ. Manage.* **2005**, 76, 135-142.
18. Amin, M.; Alazba, A.; Manzoor, U. A review of removal of pollutants from water/wastewater using different types of nanomaterials. *Adv. Mater. Sci. Eng*. **2014**, 10, 825910.
19. Nie, J.; Wang, Q.; Gao, S.; Poon, C.; Zhou, Y.; Li, Jiang-shan. Novel recycling of incinerated sewage sludge ash (ISSA) and waste bentonite as ceramsite for Pb-containing wastewater treatment: Performance and mechanism. *J. Environ. Manage*. **2021**, 288, 112382.

20. Qi, X.; Tong, P. Recent advances in polysaccharide-based adsorbents for wastewater treatment. *J. Clean. Prod*. **2021**, 315, 128221.
21. Abdullah, T.; Rasheed, R.; Juzsakova, T.; Al-Jammal, N.; Mallah, M.; P Cuong, L.; Salman, A.; Domokos, E.; Ali, Z.; Cretescu, I. Preparation and characterization of MnO_2-based nanoparticles at different annealing temperatures and their application in dye removal from water. *Int. J. Environ. Sci. Technol*. **2021**, 18, 1499-1512.
22. Hassan, F.; Faiq, F. Preparation and characterization of MWCNTs-Chitosan composite. *IOP Conf. Ser. Earth Environ. Sci*. **2021**, 790, 012008.
23. Shihad, A.; Abedalrazaq, K.; Karam, F.; Hessoon, H.; Al-Adilee, K.; Alkaim, A. New analytical method for estimation of ferrous in ferrous sulfate drug by preparation and using 2-(E-(1H_benzo (d) imidozol-2-yl) diazenyl-5-(E-4-dimethyl amino benzaliden amino) phenol as a reagent. *Int. J. Pharm. Sci. Res*. **2018**, 10, 2179-2182.
24. Jassim, T.; Haider, M.; Faiq, F. Preparation and characterization of new hetrocyclic azo thiozal dye ligand and its use as a reagent for determination of Zn^{+2} ion in drug by new analytical method. *J. Med. Chem. Sci*. **2023**, 621, 857-867.
25. Almukhtar, J.; Faiq, F. Kinetic and thermodynamic studies for mebeverine hydrochloride adsorption from aqueous solution using prepared chitosan polymer in delivery drug system. *J. Phys. Conf. Ser.* **2020**, 1664, 012062.
26. Hasan, R.; Faiq, F.; Sadiq, J. Synthesis and characterization of a novel organic reagent and its complexes with Cu(II), Cr(III), Co(III) and Fe(III) metal. *IOP Conf. Ser. Earth Environ*. *Sci.* **2022,** 1029, 012027.
27. Alzayd, A.; Faiq, F. Adsorption of Atenolol drug from Aqueous solution by poly (AAM_MA) hydrogel and used in drug delivery system: Study kinetic and thermodynamic. *Res. J. Pharm.Technol*. **2019,** 12, 4678-4682.
28. Kumar, P.; Khan, M.; Khan, R.; Ahmad, K.; Kim, H. Hydrothermal synthesis of MnO_2/reduced graphene oxide composite for 4-nitrophenol sensing applications. *Inorganics* **2022**, 10, 219.
29. Embaby, M.; Haggag, E.; El-Sheikh, A.; Marrez, D. Biosorption of Uranium from aqueous solution by green microalga *Chlorella sorokiniana*. *Environ. Sci. Pollut. Res*. **2022**, 29, 58388-58404.
30. Tara, N.; Siddiqui, S.; Bach, Q.; Chaudhry, S. Reduce graphene oxide-manganese oxide-black cumin based hybrid composite (rGO-MnO_2/BC): A novel material for water remediation. *Mater. Today Commun.* **2020**, 25, 101560.
31. Deng, S.; Sun, D.; Wu, C.; Wang, H.; Liu, J.; Sun, Y.; Yan, H. Synthesis and electrochemical properties of MnO_2 nanorods/graphene composites for supercapacitor applications. *Electrochim. Acta* **2013**, 111, 707-712.
32. Kumar, A.; Aathira, M.; Pal, U.; Jain, S. Photochemical oxidative coupling of 2-naphthols using a hybrid reduced graphene oxide/manganese dioxide nanocomposite under visible-light irradiation. *ChemCatChem.* **2018**, 10, 1844-1852.
33. Chaudhuri, H.; Niranjan, K. Heterostructured hybrid rGO@α-MnO_2/rGO@ δ-MnO_2 nanoflower: An efficient catalyst for aerobic Solvent-Free N-Alkylation reactions and energy storage material. *Chem.Cat.Chem*. **2020**, 12, 1617-1629.
34. Hasan, R.; Faiq, F. Preparation of a novel cartridge column for solid phase extraction, used for separation of some heavy metal. *J. Phys. Conf. Ser*. **2021**, 1999, 012014.
35. Shabeeb, G.; Emshary, C.; Hassan, Q.; Sultan, H. Investigating the nonlinear optical properties of poly eosin-Y phthalate solution under irradiation with low power visible CW laser light. *Physica B Condens. Matter*. **2020**, 578, 411847.
36. Hao, X.; Guo, Q.; Li, M.; Jin, Z.; Wang, Y. TiO_2 as an interfacial-charge-transfer-bridge to construct eosin Y-mediated direct Z-scheme electron transfer over a Co_9S_8 quantum dot/TiO_2 photocatalyst. *Catal. Sci. Technol.* **2020**, 10, 5267-5280.

37. Li, X.; Qing-Zhou, Z. Evaluation of eosin Y removal from aqueous solution using nano-mesoporous material MCFs: Adsorption equilibrium, kinetics, and adsorption isotherms. *Int. J. Ind. Chem.* **2020**, 11, 55-67.
38. Alwi, R.; Gopinathan, R.; Bhowal, A.; Garlapati, C. Adsorption characteristics of activated carbon for the reclamation of Eosin Y and indigo carmine colored effluents and new isotherm model. *Mol.* **2020**, 25, 6014.
39. Parveen, K.; Zafar, S.; Khan, M.; Anwer, R.; Shanableh, A. Removal of eosin yellow from wastewaters by the commercial anion exchange membrane BI. *Desalin. Water Treat*. **2023**, 287, 245-253.
40. Slyusarenko, N.; Gerasimova, M.; Atamanova, M.; Plotnikov, A. Adsorption of eosin Y on polyelectrolyte complexes based on chitosan and arabinogalactan sulfate. *Colloids Surf. A: Physicochem. Eng. Asp*. **2021**, 610, 125731.
41. Bukhari, A.; Ijaz, I.; Zain, H.; Gilani, E.; Nazir, A.; Bukhari, A.; Raza, S.; Hussain, S.; Alarfaji, S.; Naseer, Y. Removal of Eosin dye from simulated media onto lemon peel-based low cost biosorbent. *Arab. J. Chem.* **2022**, 15, 103873.
42. Lewandowska-Andra, A.; Larowska, D.; Gacka, E.; Pedzinski, T.; Marciniak, B. How Eosin Y/graphene oxide-based materials can improve efficiency of light-driven hydrogen generation: Mechanistic aspects. *J. Phys. Chem.* **2020**, 124, 2747-2755.
43. Mhammedazayd, A.; Karam, F. Kinetic and Thermodynamic studies for ciprofloxacin adsorption from aqueous solution using poly (AAM_MA) in controlled release system. *Eurasian Chem.-Technol. J.* **2018**, 20, 169-177.
44. de Freitas, C.; Estev, B.; Pellosi, D.; Scarminio, I.; Caetano, W.; Hioka, N.; Batistela, V. Chemical equilibria of Eosin Y and its synthetic ester derivatives in non-ionic and ionic micellar environments. *J. Mol. Liq.* **2021**, 327, 114794.
45. Zou, W.; Song, M.; He, J.; Qiu, P.; Sun, Z.; Su, Z.; Bai, Y. A resonance Rayleigh scattering and fluorescence quenching dual-channel sensor for sensitive detection of chitosan based on Eosin Y. *Anal. Bioanal. Chem*. **2021**, 413, 1429-1440.
46. Das, B.; Devi, M.; Hassan Barbhuiya, M.; Sankar Dhar, S. Sodium and sulfur co-doped graphitic carbon nitride: A novel and effective visible light driven photocatalyst with tunable bandgap for degradation of Eosin yellow. *ChemistrySelect*. **2020**, 5, 12190-12197.
47. Tella, A.; Bamgbose, J.; Adimula, V.; Omotoso, M.; Elaigwu, S.; Olayemi, V.; Odunola, O. Synthesis of metal–organic frameworks (MOFs) MIL-100 (Fe) functionalized with thioglycolic acid and ethylenediamine for removal of Eosin B dye from aqueous solution. *SN Appl. Sci.* **2021**, 3, 1-15.
48. Mohamadpour, F. A new role for photoexcited Na_2 eosin Y as direct hydrogen atom transfer (HAT) photocatalyst in photochemical synthesis of dihydropyran [2,3-c] pyrazole scaffolds promoted by visible light irradiation under air atmosphere. *JPPA* **2021**, 418, 113428.
49. Khan, J.; Sayed, M.; Shah, N.; Khan, S.; Zhang, Y.; Boczkaj, G.; Khan, H.; Dionysiou, D. Synthesis of eosin modified TiO_2 film with co-exposed {001} and {101} facets for photocatalytic degradation of para-aminobenzoic acid and solar H_2 production. *Appl. Catal. B: Environ*. **2020**, 265, 118557.
50. El Mitwalli, O.; Barakat, O.; Daoud, R.; Akhtar, S.; Henari, F. Green synthesis of gold nanoparticles using cinnamon bark extract, characterization, and fluorescence activity in Au/eosin Y assemblies *J. Nanoparticle Res*. **2020**, 22, 1-9.